

K2-287b: an Eccentric Warm Saturn transiting a G-dwarf

ANDRÉS JORDÁN,^{1,2} RAFAEL BRAHM,^{3,1,2} NÉSTOR ESPINOZA,^{4,*} CRISTIÁN CORTÉS,⁵ MATÍAS DÍAZ,⁶ HOLGER DRASS,^{2,3}
THOMAS HENNING,⁴ JAMES S. JENKINS,⁶ MATÍAS I. JONES,⁷ MARKUS RABUS,^{3,4} FELIPE ROJAS,¹ PAULA SARKIS,⁴
MAJA VUČKOVIĆ,⁸ ABNER ZAPATA,³ MARITZA G. SOTO,⁹ GÁSPÁR Á. BAKOS,^{10,†} DANIEL BAYLISS,¹¹ WAQAS BHATTI,¹⁰
ZOLTAN CSUBRY,¹⁰ REGIS LACHAUME,^{3,4} VÍCTOR MORAGA,¹ BLAKE PANTOJA,⁶ DAVID OSIP,¹² AVI SHPORER,¹³
VINCENT SUC,¹ AND SERGIO VÁSQUEZ¹⁴

¹*Instituto de Astrofísica, Pontificia Universidad Católica de Chile, Av. Vicuña Mackenna 4860, Macul, Santiago, Chile*

²*Millennium Institute for Astrophysics, Chile*

³*Center of Astro-Engineering UC, Pontificia Universidad Católica de Chile, Av. Vicuña Mackenna 4860, 7820436 Macul, Santiago, Chile*

⁴*Max-Planck-Institut für Astronomie, Königstuhl 17, Heidelberg 69117, Germany*

⁵*Departamento de Física, Facultad de Ciencias Básicas, Universidad Metropolitana de la Educación, Av. José Pedro Alessandri 774, 7760197, Nuñoa, Santiago, Chile*

⁶*Departamento de Astronomía, Universidad de Chile, Camino El Observatorio 1515, Las Condes, Santiago, Chile*

⁷*European Southern Observatory, Casilla 19001, Santiago, Chile*

⁸*Instituto de Física y Astronomía, Universidad de Valparaíso, Casilla 5030, Valparaíso, Chile*

⁹*School of Physics and Astronomy, Queen Mary, University of London, 327 Mile End Road, London, UK*

¹⁰*Department of Astrophysical Sciences, Princeton University, NJ 08544, USA*

¹¹*Department of Physics, University of Warwick, Coventry CV4 7AL, UK*

¹²*Las Campanas Observatory, Carnegie Institution of Washington, Colina el Pino, Casilla 601 La Serena, Chile*

¹³*Department of Physics, and Kavli Institute for Astrophysics and Space Research, Massachusetts Institute of Technology, Cambridge, MA 02139, USA*

¹⁴*Museo Interactivo Mirador, Dirección de Educación, Av. Punta Arenas 6711, La Granja, Santiago, Chile*

(Received; Revised; Accepted)

Submitted to AAS

ABSTRACT

We report the discovery of K2-287b, a Saturn mass planet orbiting a G-dwarf with a period of $P \approx 15$ days. First uncovered as a candidate using K2 campaign 15 data, follow-up photometry and spectroscopy were used to determine a mass of $M_P = 0.317 \pm 0.026 M_J$, radius $R_P = 0.833 \pm 0.013 R_J$, period $P = 14.893291 \pm 0.000025$ days and eccentricity $e = 0.476 \pm 0.026$. The host star is a metal-rich $V = 11.410 \pm 0.129$ mag G dwarf for which we estimate a mass $M_\star = 1.056^{+0.022}_{-0.021} M_\odot$, radius $R_\star = 1.070 \pm 0.010 R_\odot$, metallicity $[\text{Fe}/\text{H}] = 0.20 \pm 0.05$ and $T_{\text{eff}} = 5673 \pm 75$ K. This warm eccentric planet with a time-averaged equilibrium temperature of $T_{\text{eq}} \approx 800$ K adds to the small sample of giant planets orbiting nearby stars whose structure is not expected to be affected by stellar irradiation. Follow-up studies on the K2-287 system could help in constraining theories of migration of planets in close-in orbits.

Keywords: planetary systems – stars: individual: K2-287 – planets and satellites: gaseous planets – planets and satellites: detection

1. INTRODUCTION

Giant extrasolar planets that orbit their host stars at distances shorter than ≈ 1 AU but farther away than the hot-Jupiter pile-up at ≈ 0.1 AU, are termed “warm” giants. They have been efficiently discovered by radial velocity (RV) surveys (e.g., Hébrard et al. 2016; Jenkins et al. 2017), and have a wide distribution for their eccentricities, with a median of ≈ 0.25 . The origin for these

Corresponding author: Andrés Jordán
ajordan@astro.puc.cl

* Bernoulli fellow; Gruber fellow

† MTA Distinguished Guest Fellow, Konkoly Observatory, Hungary

eccentricities is a topic of active research because the migration of planets through interactions with the protoplanetary disc predicts circular orbits (Dunhill et al. 2013), while planet-planet scattering after disc dispersal at typical warm giant orbital distances should generate usually planet collisions rather than high eccentricity excitations (Petrovich et al. 2014).

Transiting giants are key for constraining theories of orbital evolution of exoplanets. Besides providing the true mass of the planet, follow-up observations can be carried out to constrain the sky-projected spin-orbit angle (obliquity) of the system, which is a tracer of the migration history of the planet (e.g., Zhou et al. 2015; Esposito et al. 2017; Mancini et al. 2018). While the obliquity for hot giant ($P < 10$ d) systems can be affected by strong tidal interactions (Triaud et al. 2013; Dawson 2014), the periastra of warm giants are large enough that significant changes in the spin of the outer layers of the star are avoided, and thus the primordial obliquity produced by the migration mechanism should be conserved.

Unfortunately, the number of known transiting warm giants around nearby stars is still very low. In addition to the scaling of the transit probability as a^{-1} , the photometric detection of planets with $P > 10$ days requires a high duty cycle, which puts strong limitations on the ability of ground-based wide-angle photometric surveys (e.g., Bakos et al. 2004; Pollacco et al. 2006; Bakos et al. 2013) to discover warm giants. From the total of ≈ 250 transiting giant planets detected from the ground, only 5 have orbital periods longer than 10 d (Kovács et al. 2010; Howard et al. 2012; Lendl et al. 2014; Brahm et al. 2016a; Hellier et al. 2017). On the other hand, the *Kepler* and *CoRoT* space missions found dozens of warm giants (e.g. Deeg et al. 2010; Bonomo et al. 2010; Dawson et al. 2012; Borsato et al. 2014), but orbiting mostly faint stars, for which detailed follow-up observations are very challenging.

Due to their relatively low equilibrium temperatures ($T_{\text{eq}} < 1000$ K), transiting warm giants are important objects for characterizing the internal structure of extrasolar giant planets since their atmospheres are not subject to the yet unknown mechanisms that inflate the radii of typical hot Jupiters (for a review see Fortney & Nettelmann 2010). For warm giants, standard models of planetary structure can be used to infer their internal composition from mass and radii measurements (e.g., Thorngren et al. 2016).

In this work we present the discovery of an eccentric warm giant planet orbiting a bright star, having physical parameters similar to those of Saturn. This discovery was made in the context of the K2CL collaboration,

which has discovered a number of planetary systems using K2 data (Brahm et al. 2016b; Espinoza et al. 2017; Jones et al. 2017; Giles et al. 2018; Soto et al. 2018; Brahm et al. 2018a,b).

2. OBSERVATIONS

2.1. K2

Observations of campaign 15 (field centered at RA=15:34:28 and DEC=-20:04:44) of the K2 mission (Howell et al. 2014) took place between August 23 and November 20 of 2017. The data of K2 campaign 15 was released on March 2018. We followed the steps described in previous K2CL discoveries to process the light curves and identify transiting planet candidates. Briefly, the K2 light curves for Campaign 15 were detrended using our implementation of the EVEREST algorithm (Luger et al. 2016), and a Box-Least-Squares (BLS; Kovács et al. 2002) algorithm was used to find candidate box-shaped signals. The candidates that showed power above the noise level were then visually inspected to reject evident eclipsing binary systems and/or variable stars. We identified 23 candidates in this field. Among those candidates, K2-287 (EPIC 249451861) stood out as a high priority candidate for follow-up due to its relative long period, deep flat-bottomed transits, and bright host star ($V = 11.4$ mag). The detrended light curves of the six transits observed for K2-287 by K2 are displayed in Figure 1.

2.2. Spectroscopy

We obtained 52 R=48000 spectra between March and July of 2018 using the FEROS spectrograph (Kaufer et al. 1999) mounted on the 2.2 MPG telescope in La Silla observatory. Each spectrum achieved a signal-to-noise ratio of ≈ 90 per spectral resolution element. The instrumental drift was determined via comparison with a simultaneous fiber illuminated with a ThAr+Ne lamp. We obtained additionally 25 R=115000 spectra between March and August of 2018 using the HARPS spectrograph (Mayor et al. 2003). Typical signal-to-noise ratio for these spectra ranged between 30 and 50 per spectral resolution element. Both FEROS and HARPS data were processed with the CERES suite of echelle pipelines (Brahm et al. 2017a), which produce radial velocities and bisector spans in addition to reduced spectra.

Radial velocities and bisector spans are presented in Table 3 with their corresponding uncertainties, and the radial velocities are displayed as a function of time in Figure 2. No large amplitude variations were identified which could be associated with eclipsing binary scenarios for the K2-287 system and no additional stellar components were evident in the spectra. The radial veloc-

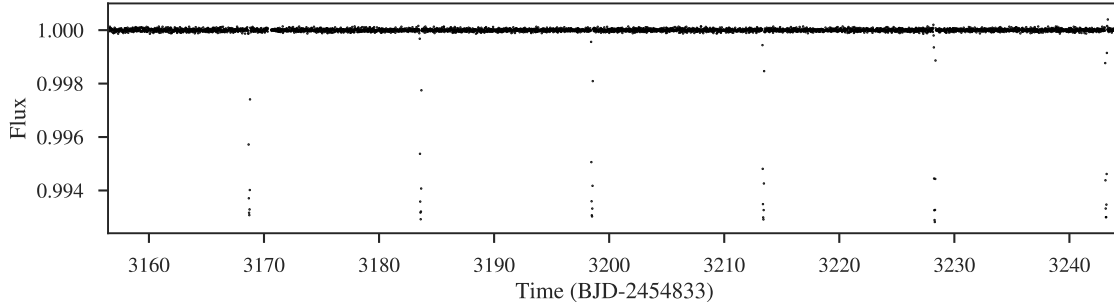


Figure 1. De-trended K2 photometry of K2-287. Black points are individual 30-min cadence K2 data. The transits of K2-287b are clearly seen.

ities present a time correlated variation in phase with the photometric ephemeris, with an amplitude consistent with the one expected to be produced by a giant planet. We find no correlation between the radial velocities and the bisector spans (95% confidence intervals for the Pearson coefficient are $[-0.19, 0.21]$, see Figure 3).

2.3. Ground-based photometry

On July 14 of 2018 we observed the primary transit of K2-287 with the Chilean-Hungarian Automated Telescope (CHAT), installed at Las Campanas Observatory, Chile. CHAT is a newly commissioned 0.7m telescope, built by members of the HATSouth (Bakos et al. 2013) team, and dedicated to the follow-up of transiting exoplanets. A more detailed account of the CHAT facility will be published at a future date (Jordán et al 2018, in prep¹). Observations were obtained in the Sloan i' band and the adopted exposure time was of 53 s per image, resulting in a peak pixel flux for K2-287 of ≈ 45000 ADU during the whole sequence. The observations covered a fraction of the bottom part of the transit and the egress (see Figure 6). The same event was also monitored by one telescope of the Las Cumbres Observatory 1m network (Brown et al. 2013) at Cerro Tololo Inter-American Observatory, Chile. Observations were obtained with the Sinistro camera with 2mm of defocus in the Sloan i band. The adopted exposure time for the 88 observations taken was 60 s, and reduced images were obtained with the standard Las Cumbres Observatory pipeline (BANZAI pipeline). The light curves for CHAT and the Las Cumbres 1m telescope were produced from the reduced images using a dedicated pipeline (Espinoza et al 2018, in prep).

The light curves were detrended by describing the systematic trends as a Gaussian Process with an exponential squared kernel depending on time, airmass and cen-

troid position and whose parameters are estimated simultaneously with those of the transit. A photometric jitter term is also included; this parameter is passed on as a fixed parameter in the final global analysis that determines the planetary parameters (§ 3.2). In more detail, the magnitude time series is modeled as

$$m_i = Z + x_1 c_{1,i} + x_2 c_{i,2} + \delta_i + \epsilon_i \quad (1)$$

where Z is a zeropoint, c_1 and c_2 are comparison light curves, x_1 and x_2 are parameters weighting the light curves, δ is the transit model and ϵ is a Gaussian Process to model the noise. The subscript i denotes evaluation at the time $t = t_i$ of the time series. For the Gaussian process, we assume a kernel given by

$$k_{ij} = A \exp \left[- \sum_m \alpha_m (x_{m,i} - x_{m,j})^2 \right] + \sigma^2 \delta_{ij}. \quad (2)$$

The variables x_m are normalized time ($m = 0$), flux centroid in x ($m = 1$) and flux centroid in y ($m = 2$); δ_{ij} is the Kronecker delta. The normalization is carried out by setting the mean to 0 and the variance to 1. The priors on the kernel hyper parameters were taken to be the same as the ones defined in Gibson (2014), the priors for the photometric jitter term σ and A were taken to be uniform in the logarithm between 0.01 and 100, with σ and A expressed in mmag. In Figure 4 we show the CHAT and LCOGT light curves with the weighted comparison stars subtracted along with the Gaussian process posterior model for the systematics.

2.4. GAIA DR2

Observations of K2-287 by GAIA were reported in DR2 (Gaia Collaboration et al. 2016, 2018). From GAIA DR2, K2-287 has a parallax of 6.29 ± 0.05 mas, an effective temperature of $T_{\text{eff}} = 4994 \pm 80$ K and a radius of $R_\star = 1.18 \pm 0.04 R_\odot$. We used the observed parallax for K2-287 measured by GAIA for estimating a more precise value of R_\star by combining it with the atmospheric

¹ https://www.exoplanetscience2.org/sites/default/files/submission-attachments/poster_aj.pdf

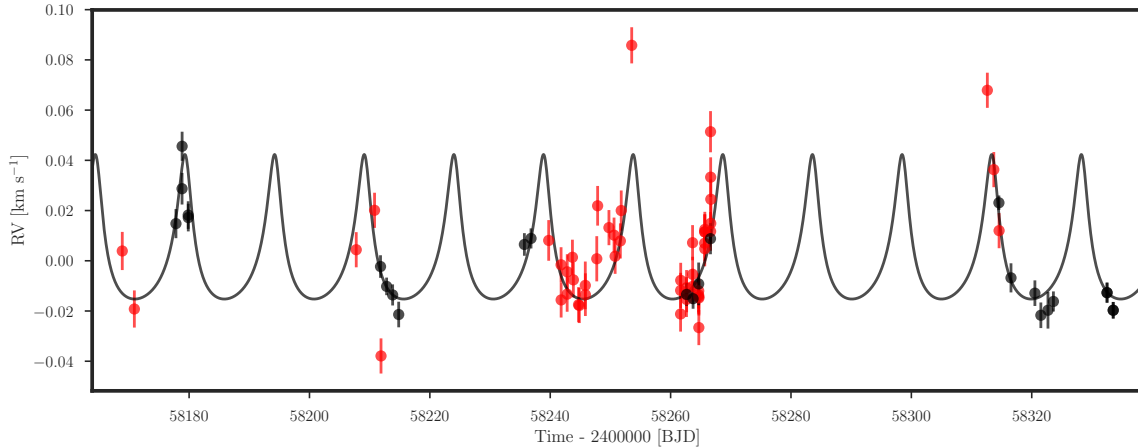


Figure 2. Radial velocity (RV) curve for K2-287 obtained with FEROS (red) and HARPS (black). The black line corresponds to the Keplerian model with the posterior parameters found in Section 3.2.

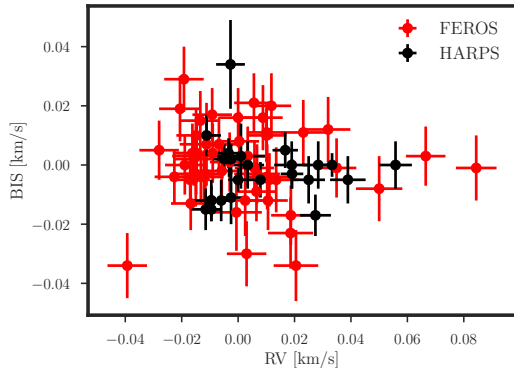


Figure 3. Radial velocity (RV) versus bisector span (BIS) scatter plot using data from our spectroscopic observations of K2-287. We find that the data is consistent with no correlation.

parameters obtained from the spectra as described in § 3. We corrected the GAIA DR2 parallax for the systematic offset of $-82 \mu\text{s}$ reported in Stassun & Torres (2018).

Two additional sources to K2-287 are identified by GAIA inside the adopted K2 aperture ($\approx 12''$). However, both stars are too faint ($\Delta G > 7.8 \text{ mag}$) to produce any significant effect on the planetary and stellar parameters found in § 3. The radial velocity variations in-phase with the transit signal, which are caused by K2-287, confirm that the transit is not caused by a blended stellar eclipsing binary on one of the companions.

3. ANALYSIS

3.1. Stellar parameters

As in previous K2CL discoveries we estimated the atmospheric parameters of the host star by comparing the co-added high resolution spectrum to a grid of synthetic

models through the ZASPE code (Brahm et al. 2017b). In particular, for K2-287 we used the co-added FEROS spectra, because they provide the higher signal-to-noise ratio spectra, and because the synthetic grid of models used by ZASPE was empirically calibrated using FEROS spectra of standard stars. Briefly, ZASPE performs an iterative search of the optimal model through χ^2 minimization on the spectral zones that are most sensitive to changes in the atmospheric parameters. The models with specific values of atmospheric parameters are generated via tri-linear interpolation of a precomputed grid generated using the ATLAS9 models (Castelli & Kurucz 2004). The interpolated model is then degraded to match the spectrograph resolution by convolving it with a Gaussian kernel that includes the instrumental resolution of the observed spectrum and an assumed macroturbulence value given by the relation presented in Valenti & Fischer (2005). The spectrum is also convolved with a rotational kernel that depends on $v \sin i$, which is considered as a free parameter. The uncertainties in the estimated parameters are obtained from Monte Carlo simulations that consider that the principal source of error comes from the systematic mismatch between the optimal model and the data, which in turn arises from poorly constrained parameters of the atomic transitions and possible deviations from solar abundances. We obtained the following stellar atmospheric parameters for K2-287: $T_{\text{eff}} = 5695 \pm 58 \text{ K}$, $\log g = 4.4 \pm 0.15 \text{ dex}$, $[\text{Fe}/\text{H}] = 0.20 \pm 0.04 \text{ dex}$, and $v \sin i = 3.2 \pm 0.2 \text{ km s}^{-1}$. The T_{eff} value obtained with ZASPE is significantly different to that reported by GAIA DR2, but is consistent that of the K2 input catalog (Huber et al. 2016).

The stellar radius is computed from the GAIA parallax measurement, the available photometry, and the atmospheric parameters. As in Brahm et al. (2018b), we used a BT-Settl-CIFIST spectral energy distribu-

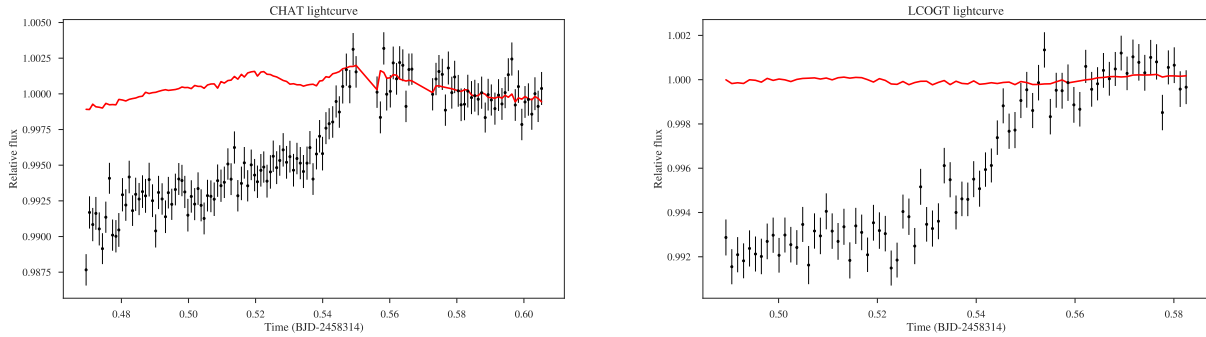


Figure 4. Ground-based light curves for the July 14 2018 transit of K2-287b obtained with CHAT (left panel) and a LCOGT 1m telescope at CTIO (right panel). The red lines represent the posterior Gaussian process models for remaining systematics after subtracting the transit and weighted comparison stars and obtained as described in §2.3

tion model (Baraffe et al. 2015) with the atmospheric parameters derived with ZASPE to generate a set of synthetic magnitudes at the distance computed from the GAIA parallax. These magnitudes are compared to those presented in table 1 for a given value of R_{\star} . We also consider an extinction coefficient A_V in our modeling which affects the synthetic magnitudes by using the prescription of Cardelli et al. (1989). We explore the parameter space for R_{\star} and A_V using the `emcee` package Foreman-Mackey et al. (2013), using uniform priors in both parameters. We found that K2-287 has a radius of $R_{\star} = 1.07 \pm 0.01 R_{\odot}$ and has a reddening of $A_V = 0.56 \pm 0.03$ mag, which is consistent with what is reported by GAIA DR2.

Finally, the stellar mass and evolutionary stage for K2-287 are obtained by comparing the estimation of R_{\star} and the spectroscopic T_{eff} with the predictions of the Yonsei-Yale evolutionary models (Yi et al. 2001). We use the interpolator provided with the isochrones to generate a model with specific values of M_{\star} , age, and $[\text{Fe}/\text{H}]$, where $[\text{Fe}/\text{H}]$ is fixed to the value found in the spectroscopic analysis. We explore the parameter space for M_{\star} and stellar age using the `emcee` package, using uniform priors in both parameters. We find that the mass and age of K2-287 are $M_{\star} = 1.036 \pm 0.033 M_{\odot}$ and 5.6 ± 1.6 Gyr (see Figure 5), similar to those of the Sun. The stellar parameters we adopted for K2-287 are summarized in Table 1.

3.2. Global modeling

In order to determine the orbital and transit parameters of the K2-287b system we performed a joint analysis of the detrended K2 photometry, the follow-up photometry, and the radial velocities. As in previous planet discoveries of the K2CL collaboration, we used the `exonailer` code which is described in detail in Espinoza et al. (2016). Briefly, we model the transit light curves using the `batman` package (Kreidberg

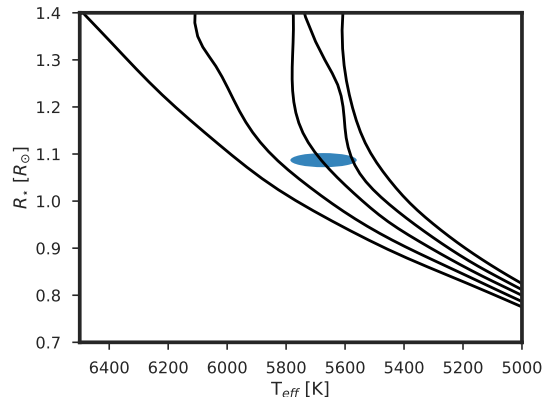


Figure 5. Yonsei-Yale isochrones for the metallicity of K2-287 in the $T_{\text{eff}}-R_{\star}$ plane. From left to right the isochrones correspond to 1, 3, 5, 7 and 9 Gyr. The position of K2-287 is at the center of the blue shaded region, which marks the 3σ confidence region for T_{eff} and R_{\star} .

2015) by taking into account the effect on the transit shape produced by the long integration time of the long-cadence K2 data (Kipping 2010). To avoid systematic biases in the determination of the transit parameters we considered the limb-darkening coefficients as additional free parameters in the transit modeling (Espinoza & Jordán 2015), with the complexity of limb-darkening law chosen following the criteria presented in Espinoza & Jordán (2016). In our case, we select the quadratic limb-darkening law, whose coefficients were fit using the uninformative sampling technique of Kipping (2013). We also include a photometric jitter parameter for the K2 data, which allow us to have an estimation of the level of stellar noise in the light curve. The radial velocities are modeled with the `radvel` package (Fulton et al. 2018), where we considered systemic velocity and jitter factors for the data of each spectrograph. We use the stellar density estimated in our stellar modeling as an extra “data point” in our global fit as described in Brahm

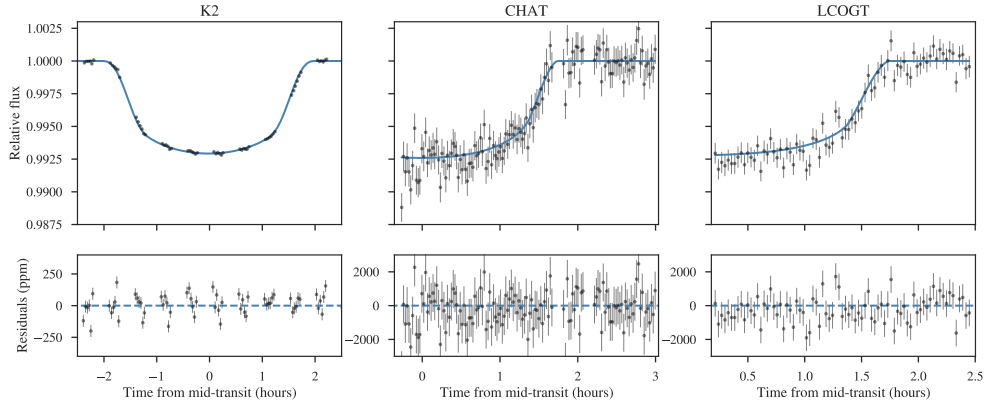


Figure 6. The top panels show from left to right: the phase folded Kepler *K2* photometry (K_p band), the CHAT follow up photometry (i band), and the LCO follow-up photometry (i band) for K2-287. For the three cases, the model generated with the derived parameters of EXONAILER is plotted with a blue line. The bottom panels show the corresponding residuals.

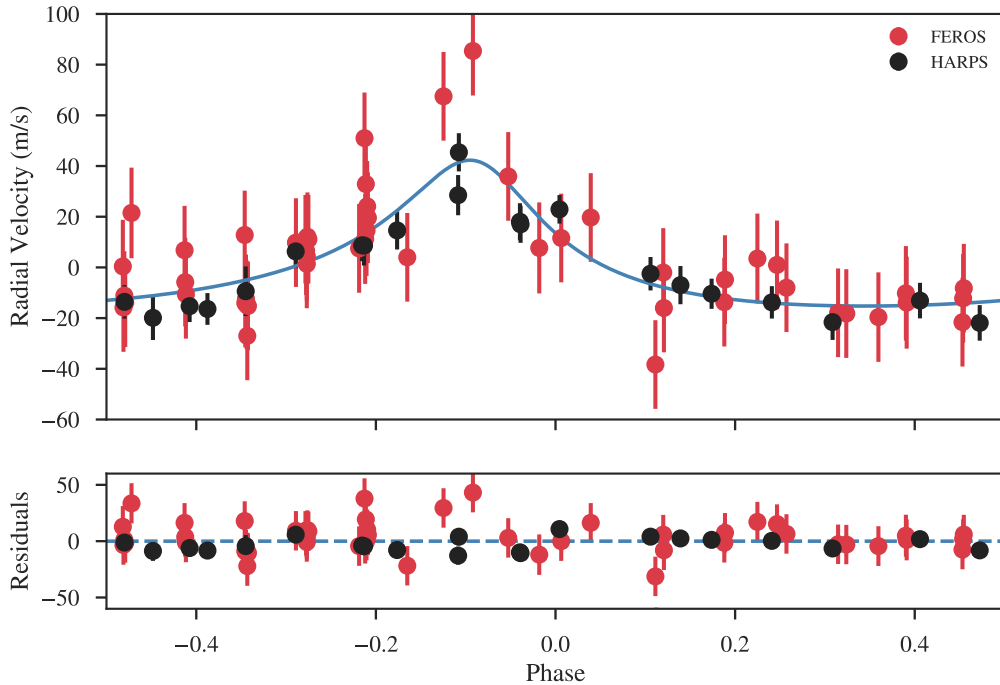


Figure 7. The top panel presents the radial velocities for K2-287 (filled circles) obtained with FEROS and HARPS as a function of the orbital phase. The RV model with the derived orbital parameters for K2-287b corresponds to the blue solid line. The bottom panel shows the residuals obtained for these radial velocity measurements.

et al. (2018a). Briefly, there is a term in the likelihood of the form

where

$$\rho_*^m = \frac{3\pi}{GP^2} \left(\frac{a}{R_*} \right)^3$$

by Newton's version of Kepler's law, and ρ_* and σ_{ρ_*} are the mean stellar density and its standard-deviation, respectively, derived from our stellar analysis. In essence, because the period P is tightly constrained by the ob-

$$p(\vec{y}_{\rho_*} | \theta) = \frac{1}{\sqrt{2\pi\sigma_{\rho_*}^2}} \exp -\frac{(\rho_* - \rho_*^m)^2}{2\sigma_{\rho_*}^2},$$

Table 1. Stellar properties of K2-287

Parameter	Value	Reference
Names	K2-287	EPIC
	2MASS J15321784-2221297	2MASS
	TYC 6196-185-1	TYCHO
	WISE J153217.84-222129.9	WISE
RA(J2000)	15h32m17.84s	EPIC
DEC(J2000)	-22d21m29.74s	EPIC
pm ^{RA} (mas yr ⁻¹)	-4.59 ± 0.11	GAIA
pm ^{DEC} (mas yr ⁻¹)	-17.899 ± 0.074	GAIA
π(mas)	6.288 ± 0.051	GAIA
K_p(mag)	11.058	EPIC
B(mag)	12.009 ± 0.169	APASS
g'(mag)	11.727 ± 0.010	APASS
V(mag)	11.410 ± 0.129	APASS
r'(mag)	11.029 ± 0.010	APASS
i'(mag)	10.772 ± 0.020	APASS
J(mag)	9.677 ± 0.023	2MASS
H(mag)	9.283 ± 0.025	2MASS
K_s(mag)	9.188 ± 0.021	2MASS
WISE1(mag)	9.114 ± 0.022	WISE
WISE2(mag)	9.148 ± 0.019	WISE
WISE3(mag)	9.089 ± 0.034	WISE
T_{eff}(K)	5695 ± 58	zaspe
log g(dex)	4.398 ± 0.015	zaspe
[Fe/H](dex)	+0.20 ± 0.04	zaspe
$v \sin i$(km s ⁻¹)	3.2 ± 0.2	zaspe
M_{\star}(M_{\odot})	1.056 ± 0.022	YY + GAIA
R_{\star}(R_{\odot})	1.07 ± 0.01	GAIA + this work
Age(Gyr)	4.5 ± 1	YY + GAIA
ρ_{\star}(g cm ⁻³)	1.217 ± 0.045	YY + GAIA

served periodic transits, this extra term puts a strong constraint on a/R_* , which in turn helps to extract information about the eccentricity e and argument of periastron ω from the duration of the transit. Resulting planet parameters are set out in Table 2, the best-fit orbit solution in Figures 2 and 7 and the best-fit light curves in Figure 6.

4. DISCUSSION

By combining data from the Kepler K2 mission and ground based photometry and spectroscopy, we have confirmed the planetary nature of a $P = 14.9$ d candidate around the $V = 11.4$ mag G-type star K2-287. We found that the physical parameters of K2-287b ($M_P = 0.317 \pm 0.026 M_J$, $R_P = 0.833 \pm 0.013 R_J$) are consistent to those of Saturn. The non-inflated structure of K2-287b is expected given its relatively low time-averaged equilibrium temperature of $T_{\text{eq}} = 808 \pm 8$ K. In Figure 8 the mass and radius of K2-287b are compared to those for the full population of transiting planets with parameters measured to a precision of 20% or better. Two other transiting planets, orbiting fainter stars, that share similar structural properties to K2-287b are HAT-P-38b (Sato et al. 2012) and HATS-20b (Bhatti et al. 2016), which have equilibrium temperatures that are higher but relatively close to the $T_{\text{eq}} \approx 1000$ K limit below which the inflation mechanism of hot Jupiters does not play a significant role (Kovács et al. 2010; Demory & Seager 2011). By using the simple planet structural models of Fortney et al. (2007) we find that the observed properties of K2-287b are consistent with having a solid core of $M_c = 31 \pm 4 M_\oplus$. However, models that consider the presence of solid material in the envelope of the planet are required to obtain a more reliable estimate for the heavy element content of K2-287b (e.g., Thorngren et al. 2016).

The numerous radial velocity measurements obtained for the K2-287 system allow us to constrain the eccentricity of the planet to be $e = 0.478 \pm 0.025$. Even though K2-287b is among the most eccentric extrasolar planets to have a period shorter than 50 days, its periastron distance is not small enough to cause a significant migration by tidal interactions throughout the main sequence lifetime of the host star. Specifically, by using the equations of Jackson et al. (2009), we find that in the absence of external sources of gravitational interaction, K2-287b should have possessed an eccentricity of $e \approx 0.65$ and a semi-major axis of $a \approx 0.15$ AU when the system was 0.1 Gyr old. Under the same assumptions, we expect that K2-287b would be engulfed by its host star at an age of ≈ 12 Gyr before being able to reach full circularization at a distance of $a \approx 0.1$ AU. These orbital properties for

K2-287b and those of the majority of eccentric warm giants are not easy to explain. If K2-287b was formed *in situ* (Huang et al. 2016) at 0.15 AU or migrated to this position via interactions with the protoplanetary disc (Lin & Ida 1997), its eccentricity could have been excited by the influence of another massive object in the system after disc dispersal. However, planet-planet scattering (Ford & Rasio 2008) at these close-in orbits generally produces planet collisions rather than eccentricity excitation (Petrovich et al. 2014). An alternative proposition for the existence of these eccentric systems is that they are being subject to secular gravitational interactions produced by another distant planet or star in the system (Rasio & Ford 1996), with the planet experiencing long term cyclic variations in its eccentricity and spin orbit angle. In this scenario, the planet migrates by tidal interactions only during the high eccentricity stages, but it is usually found with moderate eccentricities. Further observations on the K2-287 system could help support this mechanism as the responsible for its relatively high eccentricity, particularly given that Petrovich & Tremaine (2016) concludes that high-eccentricity migration excited by an outer planetary companion can account for most of the warm giants with $e > 0.4$. Specifically, long term radial velocity monitoring and the search for transit timing variations could be used to detect the relatively close companions to migrating warm Jupiters proposed by Dong et al. (2014). Future astrometric searches of companions with GAIA could also be used to find companions and infer the predicted mutual inclination between both orbits, which are predicted to be high Anderson & Lai (2017).

Finally, it is worth noting that an important fraction of the transiting warm giants amenable for detailed characterization ($J < 11$ mag) have been discovered in the last couple of years thanks to the K2 mission (see Figure 9). The combination of relatively long observing campaigns per field, and the increased number of fields monitored, have allowed the discovery and dynamical characterization of several warm giant planets with data from the K2 mission (see Figure 9, Simukoff et al. 2016; Smith et al. 2017; Barragán et al. 2017; Shporer et al. 2017; Brahm et al. 2018a; Yu et al. 2018; Brahm et al. 2018b; Johnson et al. 2018). While not particularly designed to discover warm giants, the TESS mission (Ricker et al. 2015) is expected to discover ≈ 120 additional warm giants with $R_P > 4R_\oplus$ and an incident flux $F < 150F_\oplus$, where F_\oplus is the incident flux at Earth, around $J \lesssim 11$ mag stars (Barclay et al. 2018). With such population at hand, it will be possible to compare the distributions of eccentricities and obliquities to predictions from different migration mechanisms

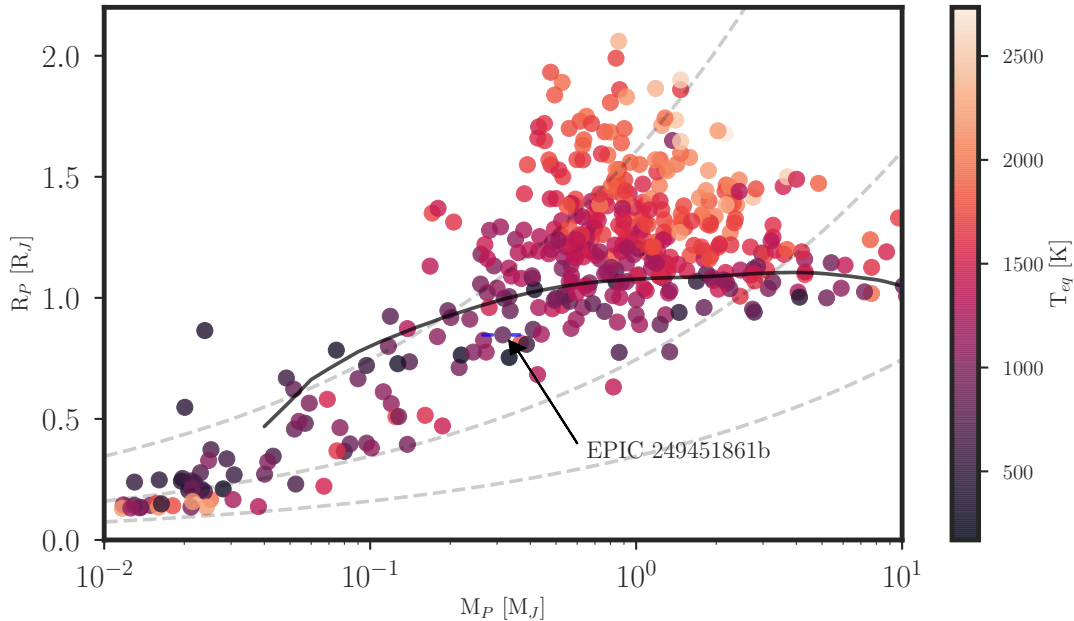


Figure 8. Mass-Radius diagram for the full population of transiting planets with both parameters measured to at least 20% precision. The points are color-coded by equilibrium temperature. K2-287b is the object in the plot that has error bars and is indicated by the arrow. The dashed gray lines correspond to iso-density curves of 0.3 , 3 , and 30 g cm^{-3} , while the solid line represents the prediction of the Fortney et al. (2007) structural model with a central core mass of $10 M_{\oplus}$. Due to its relatively low equilibrium temperature, K2-287b lies in a sparsely populated region of the parameter space of moderately compact giant planets.

(e.g. Petrovich & Tremaine 2016) in order to establish a clearer picture about how eccentric warm giant planets originate.

A.J. acknowledges support from FONDECYT project 1171208, CONICYT project BASAL AFB-170002, and by the Ministry for the Economy, Development, and Tourism’s Programa Iniciativa Científica Milenio through grant IC120009, awarded to the Millennium Institute of Astrophysics (MAS). R.B. acknowledges support from FONDECYT Post-doctoral Fellowship Project 3180246, and from the Millennium Institute of Astrophysics (MAS). M.R.D. acknowledges support by CONICYT-PFCHA/Doctorado Nacional 21140646, Chile. A.Z. acknowledges support by CONICYT-PFCHA/Doctorado Nacional 21170536, Chile. J.S.J. acknowledges support by FONDECYT project 1161218 and partial support by CONICYT project BASAL AFB-170002. This paper includes data collected by the K2 mission. Funding for the K2 mission is provided by the

NASA Science Mission directorate. This work has made use of data from the European Space Agency (ESA) mission Gaia (<https://www.cosmos.esa.int/gaia>), processed by the Gaia Data Processing and Analysis Consortium (DPAC, <https://www.cosmos.esa.int/web/gaia/dpac/consortium>). Funding for the DPAC has been provided by national institutions, in particular the institutions participating in the Gaia Multilateral Agreement. Based on observations collected at the European Organisation for Astronomical Research in the Southern Hemisphere under ESO programmes 0101.C-0497, 0101.C-0407, 0101.C-0510.

Facilities: CHAT 0.7m, LCOGT 1m, MPG 2.2m, ESO 3.6m, *Kepler*, GAIA, APASS, 2MASS, WISE

Software: EXO-NAILER (Espinoza et al. 2016), CERES (Brahm et al. 2017a; Jordán et al. 2014), ZASPE (Brahm et al. 2017b, 2015), radvel (Fulton et al. 2018)

REFERENCES

Anderson, K. R., & Lai, D. 2017, MNRAS, 472, 3692

Bakos, G., Noyes, R. W., Kovács, G., et al. 2004, PASP, 116, 266

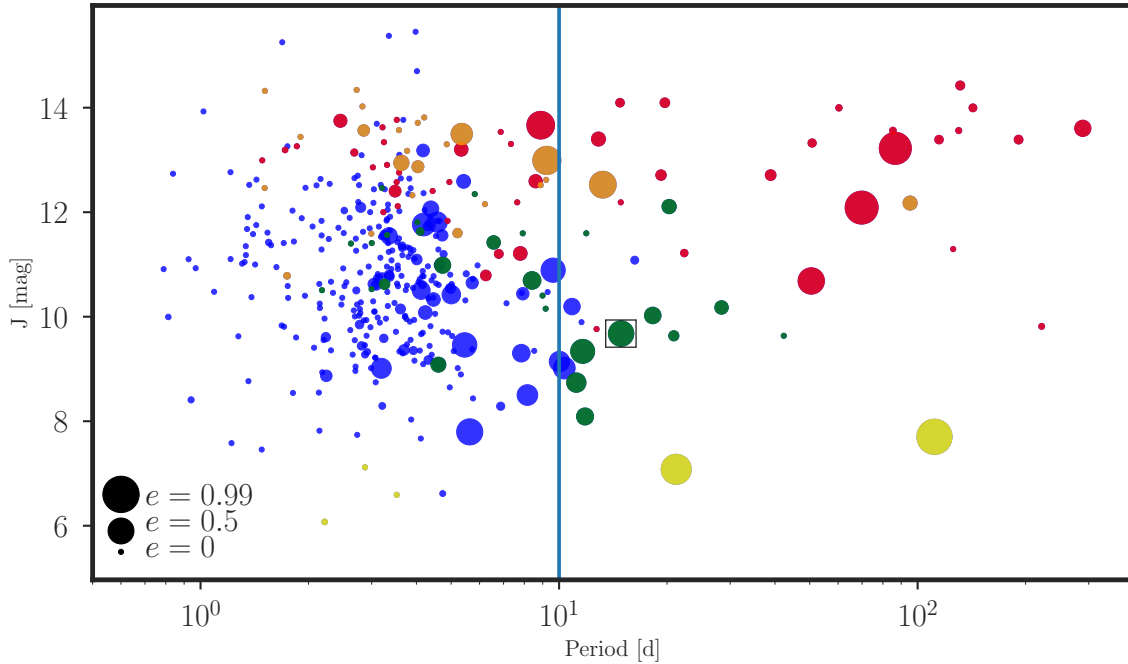


Figure 9. Population of well characterized giant planets having $R_p > 0.4 R_J$ in the orbital period – J magnitude plane. K2-287b is inside a black square. The size of the points represent the eccentricity of the orbit, while the color indicates the discovery method/mission (blue: ground-based photometry, yellow: RV planets, orange: CoRoT, red: *Kepler*, green: *Kepler* K2). The *Kepler* K2 mission has been the most effective source for discovering transiting bright ($J < 11$) warm ($P > 10$ d) giant planets.

- Bakos, G. Á., Csubry, Z., Penev, K., et al. 2013, *PASP*, 125, 154
- Baraffe, I., Homeier, D., Allard, F., & Chabrier, G. 2015, *A&A*, 577, A42
- Barclay, T., Pepper, J., & Quintana, E. V. 2018, *ArXiv e-prints*, arXiv:1804.05050
- Barragán, O., Gandolfi, D., Dai, F., et al. 2017, *ArXiv e-prints*, arXiv:1711.02097
- Bhatti, W., Bakos, G. Á., Hartman, J. D., et al. 2016, *ArXiv e-prints*, arXiv:1607.00322
- Bonomo, A. S., Santerne, A., Alonso, R., et al. 2010, *A&A*, 520, A65
- Borsato, L., Marzari, F., Nascimbeni, V., et al. 2014, *A&A*, 571, A38
- Brahm, R., Jordán, A., & Espinoza, N. 2017a, *PASP*, 129, 034002
- Brahm, R., Jordán, A., Hartman, J., & Bakos, G. 2017b, *MNRAS*, 467, 971
- Brahm, R., Jordán, A., Hartman, J. D., et al. 2015, *AJ*, 150, 33
- Brahm, R., Jordán, A., Bakos, G. Á., et al. 2016a, *AJ*, 151, 89
- Brahm, R., Jones, M., Espinoza, N., et al. 2016b, *PASP*, 128, 124402
- Brahm, R., Espinoza, N., Jordán, A., et al. 2018a, *MNRAS*, 477, 2572
- Brahm, R., Espinoza, N., Rabus, M., et al. 2018b, *ArXiv e-prints*, arXiv:1806.04073
- Brown, T. M., Baliber, N., Bianco, F. B., et al. 2013, *Publications of the Astronomical Society of the Pacific*, 125, 1031
- Cardelli, J. A., Clayton, G. C., & Mathis, J. S. 1989, *ApJ*, 345, 245
- Castelli, F., & Kurucz, R. L. 2004, *ArXiv e-prints*, astro
- Dawson, R. I. 2014, *ApJL*, 790, L31
- Dawson, R. I., Johnson, J. A., Morton, T. D., et al. 2012, *ApJ*, 761, 163
- Deeg, H. J., Moutou, C., Erikson, A., et al. 2010, *Nature*, 464, 384
- Demory, B.-O., & Seager, S. 2011, *ApJS*, 197, 12
- Dong, S., Katz, B., & Socrates, A. 2014, *ApJL*, 781, L5
- Dunhill, A. C., Alexander, R. D., & Armitage, P. J. 2013, *MNRAS*, 428, 3072
- Espinoza, N., & Jordán, A. 2015, *MNRAS*, 450, 1879
- . 2016, *MNRAS*, 457, 3573
- Espinoza, N., Brahm, R., Jordán, A., et al. 2016, *ApJ*, 830, 43
- Espinoza, N., Rabus, M., Brahm, R., et al. 2017, *MNRAS*, 471, 4374
- Esposito, M., Covino, E., Desidera, S., et al. 2017, *A&A*, 601, A53
- Ford, E. B., & Rasio, F. A. 2008, *ApJ*, 686, 621

Table 2. Planetary properties of the K2-287 system. For the priors, $N(\mu, \sigma)$ stands for a normal distribution with mean μ and standard deviation σ , $U(a, b)$ stands for a uniform distribution between a and b , and $J(a, b)$ stands for a Jeffrey’s prior defined between a and b .

Parameter	Prior	Value
P (days)	$N(14.893, 0.01)$	14.893291 ± 0.000025
T_0 (BJD)	$N(2458001.722, 0.01)$	$2458001.72138 \pm 0.00016$
a/R_\star	$U(1, 300)$	$23.87^{+0.30}_{-0.31}$
R_P/R_\star	$U(0.001, 0.5)$	$0.08014^{+0.00086}_{-0.00098}$
σ_w^{K2} (ppm)	$J(10, 50000)$	$47.7^{+0.54}_{-0.54}$
q_1^{K2}	$U(0, 1)$	$0.32^{+0.06}_{-0.05}$
q_2^{K2}	$U(0, 1)$	$0.57^{+0.13}_{-0.11}$
q_1^{CHAT}	$U(0, 1)$	$0.83^{+0.12}_{-0.17}$
q_2^{CHAT}	$U(0, 1)$	$0.15^{+0.16}_{-0.11}$
q_1^{LCO}	$U(0, 1)$	$0.62^{+0.20}_{-0.19}$
q_2^{LCO}	$U(0, 1)$	$0.08^{+0.11}_{-0.06}$
K (m s^{-1})	$N(0, 100)$	$28.8^{+2.3}_{-2.2}$
e	$U(0, 1)$	$0.478^{+0.025}_{-0.026}$
i (deg)	$U(0, 90)$	$88.13^{+0.1}_{-0.08}$
ω (deg)	$U(0, 360)$	$10.1^{+4.6}_{-4.2}$
γ_{FEROS} (m s^{-1})	$N(32963.2, 0.1)$	$32930.41^{+0.10}_{-0.10}$
γ_{HARPS} (m s^{-1})	$N(32930.4, 0.1)$	$32963.19^{+0.10}_{-0.10}$
σ_{FEROS} (m s^{-1})	$J(0.1, 100)$	$16.0^{+2.1}_{-1.8}$
σ_{HARPS} (m s^{-1})	$J(0.1, 100)$	$4.8^{+1.8}_{-1.6}$
M_P (M_J)		0.315 ± 0.027
R_P (R_J)		0.847 ± 0.013
a (AU)		$0.1206^{+0.0008}_{-0.0008}$
T_{eq}^a (K)		804^{+8}_{-7}

^aTime-averaged equilibrium temperature computed according to equation 16 of Méndez & Rivera-Valentín (2017)

- Foreman-Mackey, D., Hogg, D. W., Lang, D., & Goodman, J. 2013, *PASP*, 125, 306
- Fortney, J. J., Marley, M. S., & Barnes, J. W. 2007, *ApJ*, 659, 1661
- Fortney, J. J., & Nettelmann, N. 2010, *SSRv*, 152, 423
- Fulton, B. J., Petigura, E. A., Blunt, S., & Sinukoff, E. 2018, *ArXiv e-prints*, arXiv:1801.01947
- Gaia Collaboration, Brown, A. G. A., Vallenari, A., et al. 2018, *ArXiv e-prints*, arXiv:1804.09365
- Gaia Collaboration, Prusti, T., de Bruijne, J. H. J., et al. 2016, *A&A*, 595, A1
- Gibson, N. P. 2014, *MNRAS*, 445, 3401
- Giles, H. A. C., Bayliss, D., Espinoza, N., et al. 2018, *MNRAS*, 475, 1809
- Hébrard, G., Arnold, L., Forveille, T., et al. 2016, *A&A*, 588, A145
- Hellier, C., Anderson, D. R., Cameron, A. C., et al. 2017, *MNRAS*, 465, 3693
- Howard, A. W., Bakos, G. Á., Hartman, J., et al. 2012, *ApJ*, 749, 134
- Howell, S. B., Sobek, C., Haas, M., et al. 2014, *Publications of the Astronomical Society of the Pacific*, 126, 398
- Huang, C., Wu, Y., & Triaud, A. H. M. J. 2016, *ApJ*, 825, 98
- Huber, D., Bryson, S. T., Haas, M. R., et al. 2016, *ApJS*, 224, 2
- Jackson, B., Barnes, R., & Greenberg, R. 2009, *ApJ*, 698, 1357
- Jenkins, J. S., Jones, H. R. A., Tuomi, M., et al. 2017, *MNRAS*, 466, 443
- Johnson, M. C., Dai, F., Justesen, A. B., et al. 2018, *MNRAS*, arXiv:1806.06099
- Jones, M. I., Brahm, R., Espinoza, N., et al. 2017, *ArXiv e-prints*, arXiv:1707.00779
- Jordán, A., Brahm, R., Bakos, G. Á., et al. 2014, *AJ*, 148, 29
- Kaufer, A., Stahl, O., Tubbesing, S., et al. 1999, *The Messenger*, 95, 8
- Kipping, D. M. 2010, *MNRAS*, 408, 1758
- . 2013, *MNRAS*, 435, 2152
- Kovács, G., Zucker, S., & Mazeh, T. 2002, *A&A*, 391, 369
- Kovács, G., Bakos, G. Á., Hartman, J. D., et al. 2010, *ApJ*, 724, 866
- Kreidberg, L. 2015, *PASP*, 127, 1161
- Lendl, M., Triaud, A. H. M. J., Anderson, D. R., et al. 2014, *A&A*, 568, A81
- Lin, D. N. C., & Ida, S. 1997, *ApJ*, 477, 781
- Luger, R., Agol, E., Kruse, E., et al. 2016, *AJ*, 152, 100
- Mancini, L., Esposito, M., Covino, E., et al. 2018, *A&A*, 613, A41
- Mayor, M., Pepe, F., Queloz, D., et al. 2003, *The Messenger*, 114, 20
- Méndez, A., & Rivera-Valentín, E. G. 2017, *ApJL*, 837, L1
- Petrovich, C., & Tremaine, S. 2016, *ApJ*, 829, 132
- Petrovich, C., Tremaine, S., & Rafikov, R. 2014, *ApJ*, 786, 101
- Pollacco, D. L., Skillen, I., Collier Cameron, A., et al. 2006, *PASP*, 118, 1407
- Rasio, F. A., & Ford, E. B. 1996, *Science*, 274, 954
- Ricker, G. R., Winn, J. N., Vanderspek, R., et al. 2015, *Journal of Astronomical Telescopes, Instruments, and Systems*, 1, 014003
- Sato, B., Hartman, J. D., Bakos, G. Á., et al. 2012, *PASJ*, 64, 97
- Shporer, A., Zhou, G., Fulton, B. J., et al. 2017, *AJ*, 154, 188
- Sinukoff, E., Howard, A. W., Petigura, E. A., et al. 2016, *ApJ*, 827, 78
- Smith, A. M. S., Gandolfi, D., Barragán, O., et al. 2017, *MNRAS*, 464, 2708
- Soto, M. G., Díaz, M. R., Jenkins, J. S., et al. 2018, *ArXiv e-prints*, arXiv:1801.07959
- Stassun, K. G., & Torres, G. 2018, *ApJ*, 862, 61
- Thorngren, D. P., Fortney, J. J., Murray-Clay, R. A., & Lopez, E. D. 2016, *ApJ*, 831, 64
- Triaud, A. H. M. J., Anderson, D. R., Collier Cameron, A., et al. 2013, *A&A*, 551, A80
- Valenti, J. A., & Fischer, D. A. 2005, *ApJS*, 159, 141
- Yi, S., Demarque, P., Kim, Y.-C., et al. 2001, *ApJS*, 136, 417
- Yu, L., Rodriguez, J. E., Eastman, J. D., et al. 2018, *ArXiv e-prints*, arXiv:1803.02858
- Zhou, G., Bayliss, D., Hartman, J. D., et al. 2015, *ApJL*, 814, L16

APPENDIX

Table 3. Relative radial velocities and bisector spans for K2-287.

BJD (2,400,000+)	RV (m s ⁻¹)	σ_{RV} (m s ⁻¹)	BIS (m s ⁻¹)	σ_{BIS} (m s ⁻¹)	Instrument
58168.8957118	32.9339	0.0076	-0.033	0.012	FEROS
58170.9025854	32.9108	0.0074	-0.002	0.011	FEROS
58177.8140231	32.9778	0.0058	-0.014	0.008	HARPS
58178.8260537	32.9917	0.0063	-0.014	0.008	HARPS
58178.8381972	33.0086	0.0058	-0.009	0.008	HARPS
58179.8509201	32.9812	0.0055	-0.009	0.008	HARPS
58179.8616916	32.9802	0.0055	-0.026	0.007	HARPS
58207.7691953	32.9344	0.0070	-0.051	0.011	FEROS
58210.8120326	32.9501	0.0070	-0.038	0.010	FEROS
58211.8033524	32.9607	0.0045	-0.014	0.006	HARPS
58211.8839384	32.8921	0.0070	-0.055	0.011	FEROS
58211.8969659	32.8463	0.0083	-0.100	0.012	FEROS
58212.8162559	32.9528	0.0035	-0.014	0.004	HARPS
58213.8155843	32.9494	0.0042	-0.005	0.005	HARPS
58214.8225570	32.9416	0.0051	0.001	0.007	HARPS
58235.7054437	32.9695	0.0045	-0.004	0.006	HARPS
58236.8070269	32.9719	0.0040	-0.012	0.005	HARPS
58239.7443848	32.9381	0.0081	-0.024	0.010	FEROS
58241.8009423	32.9284	0.0070	-0.020	0.010	FEROS
58241.8119744	32.9144	0.0070	-0.026	0.010	FEROS
58242.8136144	32.9167	0.0070	-0.017	0.010	FEROS
58242.8246191	32.9256	0.0070	-0.023	0.010	FEROS
58243.6877674	32.9314	0.0070	-0.005	0.010	FEROS
58243.8443690	32.9224	0.0070	-0.017	0.010	FEROS
58244.7006355	32.9125	0.0070	-0.021	0.010	FEROS
58244.8366538	32.9122	0.0070	0.008	0.011	FEROS
58245.8250104	32.9202	0.0095	-0.014	0.014	FEROS
58245.8380679	32.9165	0.0085	-0.018	0.013	FEROS
58247.7318034	32.9308	0.0090	-0.037	0.013	FEROS
58247.8756418	32.9519	0.0079	-0.055	0.012	FEROS
58249.7532000	32.9432	0.0070	-0.001	0.011	FEROS
58250.7827423	32.9318	0.0070	-0.013	0.010	FEROS
58250.6025575	32.9402	0.0070	-0.005	0.011	FEROS
58251.6502971	32.9379	0.0070	-0.030	0.010	FEROS
58251.7959960	32.9500	0.0080	-0.044	0.012	FEROS
58253.5376199	33.0158	0.0072	-0.022	0.011	FEROS
58261.6566471	32.9088	0.0070	-0.025	0.009	FEROS
58261.6676712	32.9182	0.0070	-0.025	0.009	FEROS
58261.6786827	32.9222	0.0070	-0.004	0.009	FEROS
58262.6356569	32.9146	0.0070	-0.034	0.009	FEROS
58262.6501525	32.9193	0.0070	-0.025	0.009	FEROS
58262.6526217	32.9496	0.0045	-0.007	0.006	HARPS
58262.6646765	32.9165	0.0070	-0.011	0.009	FEROS
58263.6490366	32.9372	0.0070	-0.022	0.009	FEROS

58263.6600382	32.9246	0.0070	-0.014	0.009	FEROS
58263.6710446	32.9198	0.0070	-0.024	0.009	FEROS
58263.7327984	32.9479	0.0040	-0.007	0.005	HARPS
58264.6559473	32.9164	0.0070	-0.024	0.011	FEROS
58264.6629948	32.9538	0.0085	-0.006	0.011	HARPS
58264.6669743	32.9180	0.0070	-0.006	0.010	FEROS
58264.6779962	32.9157	0.0070	-0.019	0.009	FEROS
58264.6890058	32.9034	0.0070	-0.016	0.010	FEROS
58264.7000122	32.9152	0.0070	-0.017	0.010	FEROS
58265.6537546	32.9415	0.0070	-0.010	0.010	FEROS
58265.6647735	32.9370	0.0070	0.000	0.010	FEROS
58265.6757786	32.9348	0.0070	-0.018	0.010	FEROS
58265.6867851	32.9425	0.0070	-0.026	0.009	FEROS
58265.7022013	32.9415	0.0070	-0.011	0.009	FEROS
58266.6252665	32.9718	0.0062	-0.009	0.008	HARPS
58266.6331695	32.9814	0.0082	-0.029	0.011	FEROS
58266.6441948	32.9417	0.0077	-0.025	0.011	FEROS
58266.6552239	32.9633	0.0079	-0.009	0.011	FEROS
58266.6662336	32.9449	0.0078	-0.026	0.011	FEROS
58266.6772400	32.9545	0.0079	-0.010	0.011	FEROS
58312.6234698	32.9979	0.0070	-0.018	0.010	FEROS
58313.6965328	32.9663	0.0070	-0.022	0.010	FEROS
58314.5467674	32.9861	0.0029	-0.009	0.004	HARPS
58314.5754726	32.9420	0.0070	-0.033	0.010	FEROS
58316.5526131	32.9562	0.0058	-0.009	0.008	HARPS
58320.5251962	32.9501	0.0051	0.025	0.015	HARPS
58321.5156072	32.9413	0.0051	-0.024	0.007	HARPS
58322.6976017	32.9433	0.0073	-0.021	0.007	HARPS
58323.6016488	32.9468	0.0040	-0.021	0.007	HARPS
58332.5127365	32.9503	0.0040	-0.020	0.009	HARPS
58333.5353776	32.9433	0.0033	-0.021	0.005	HARPS
58332.5127365	32.9503	0.0040	-0.007	0.005	HARPS
58333.5353776	32.9433	0.0033	-0.024	0.004	HARPS
